Research Article | Vol. 27, No. 8 | 15 Apr 2019 | OPTICS EXPRESS A269
Optics EXPRESS

Optical study of back-contacted CIGS solar cells

NASIM REZAEI,[1,*] OLINDO ISABELLA,[1] PAUL PROCEL,[1] ZEGER VROON,[2] AND MIRO ZEMAN[1]

[1]*Delft University of Technology, Photovoltaic Materials and Devices Laboratory, Mekelweg 4, 2628CD Delft, Netherlands*
[2]*TNO-Brightlands Materials Center, Urmondsebaan 22, 6167 RD Geleen, PO BOX 18, 6160 MD Geleen, Netherlands*
**n.rezaei@tudelft.nl*

Abstract: A novel back-contacted solar cell based on a submicron copper indium gallium (di)selenide (CIGS) absorber is proposed and optically investigated. First, charge carrier collection feasibility is studied by band diagram analysis. Then, two back-contacted configurations are suggested and optimized for maximum current production. The results are compared with a reference front/back-contacted CIGS solar cell with a 750-nm-thick absorber. Current density production of 38.84 mA/cm^2 is predicted according to our simulations for a realistic front-side texturing. This shows more than 38% improvement in optical performance compared to the reference cell and only 7.7% deviation from the theoretical Green absorption benchmark.

1. Introduction

Reducing the absorber thickness of copper indium gallium (di)selenide (CIGS) solar cells to values below 1 μm is the key to more industrially viable thin-film solar cells [1-3]. The resulting optical losses can be compensated by advanced light management techniques. These techniques include: (i) light in-coupling [4-7], (ii) light scattering [8-10] and (iii) light trapping [3,11]. Even though the performance of ultra-thin CIGS solar cells can be improved by the abovementioned methods, there are still more challenges to overcome in this topic. Firstly, the parasitic absorption in the front layers of a submicron CIGS solar cell contributes to more than 10% of optical losses [4]. Secondly, for CIGS devices deposited on thin flexible foils [12], the metallic grid at the front side of a front/back-contacted (FBC) solar cell, blocks a significant part of the incident light from entering the cell (optical shading) [13].

In an interdigitated back-contacted (IBC) solar cell, both electron (e) and hole (h) contacts (e-contact and h-contact) are alternatively located at the rear side of the absorber, as demonstrated in a number of high efficiency c-Si IBC solar cells [14-22]. This way, the optical shading and parasitic absorption are eliminated and the high energy photons can reach the absorber bulk and contribute to charge carrier generation. In this work, we introduce an IBC CIGS solar cell with a submicron absorber thickness. The collection feasibility of both charge carriers is studied by band diagram analysis. Two light in-coupling configurations, namely, high aspect ratio front textures (see Fig. 1) and double-layer antireflection coating (ARC, see Fig. 2) will be investigated by means of rigorous three-dimensional (3D) optical simulations. In both configurations, the e-contact dimensions are optimized for maximum current generation. This study provides guidelines to CIGS research community about IBC CIGS solar cells, which to our knowledge has not been studied so far.

#353033 https://doi.org/10.1364/OE.27.00A269
Journal © 2019 Received 29 Nov 2018; revised 19 Jan 2019; accepted 28 Jan 2019; published 20 Feb 2019

Optics EXPRESS

2. Modelling platform

Sentaurus TCAD simulator [14,23,24] was used to compute the band diagram of the e- and h-contacts in equilibrium conditions. The physical parameters of each material are listed in Table 1.

Table 1. The model parameters used for band diagram modelling in TCAD software. Density of states of electrons and holes are indicated with eDOS and hDOS, respectively. Subscripts A and D stand for acceptor and donor, respectively.

Layer parameter	Symbol (unit)	CIGS [25]	ZnO:Ga (GZO) [26]	Al_2O_3 [27]
Bandgap	E_g (eV)	1-1.14 (Ga-dep)	3.25	6.4
Relative permittivity	ε_r	13.6	3.85	2.7
eDOS	N_c (cm^{-3})	6.8×10^{17}	3.7×10^{18}	-
hDOS	N_v (cm^{-3})	1.5×10^{19}	-	-
Doping	N_A or N_D (cm^{-3})	1×10^{16} (A)	3.2×10^{19}	-

The optical performance of the solar cell was modelled by using a 3D Maxwell's equation solver, called Ansys HFSS. This finite element method-based tool allows for calculating the absorptance (A) and reflectance (R) spectra of complex thin-film structures with sub-wavelength features [4,28-31]. The structure is discretized (meshed) by tetrahedrons and the Maxwell's equations are iteratively solved at each frequency until the solution reaches an acceptable level of convergence [31]. The optical constants of CIGS [28,32], Mo [28,33], ZnO:Ga (GZO) [26], MgF_2 [34] and Al_2O_3 [27] are used as modelling inputs. Master and slave boundary conditions are deployed to model the periodic structure. More details about the modelling scheme can be found in [4,28]. The current density generated in the absorber ($J_{ph\text{-}CIGS}$) or dissipated in the i-th layer of the structure ($J_{ph\text{-}i}$) was calculated by integrating the product of wavelength-dependent absorptance spectrum (A_i) with AM1.5G photon flux ($\Phi(\lambda)$ [35]):

$$J_{ph-i} = q\int_{300}^{1200} A_i(\lambda)\Phi(\lambda)d\lambda \quad (1)$$

where q is the elementary charge and i refers to the i-th different layer. Here, $J_{ph\text{-}CIGS}$ represents the short circuit current density (J_{sc}) of the solar cell, assuming full charge carrier collection. It should be noted that both transverse electric (TE) and transverse magnetic (TM) polarizations are considered in the simulations and each absorptance spectrum is the average between the related spectra obtained from the two polarizations.

Green absorption limit [36] is used as a benchmark with which the optical performance is compared. This parameter describes the maximum absorption spectrum of a randomly textured slab of a material (here, CIGS) for which (i) front reflectance is completely quenched, (ii) light propagating in it is completely randomized, and (iii) rear internal reflectance caused by a lossless metallic reflector is maximized. The Green limit is calculated as:

$$A_{Green} = \frac{1-e^{-4\alpha d}}{1-(1-1/n^2)e^{-4\alpha d}} \quad (2)$$

in which α is the absorption coefficient, d is thickness and n is refractive index of the absorbing material.

The proposed solar cell structures are compared to a reference FBC cell with a CIGS thickness of 750 nm. From the light-facing window layers to the rear contact, the cell structure comprises the following layers: ZnO:Al / i-ZnO / CdS / CIGS / Mo. More details about the optical modelling of the reference cell can be found in [4] and [28].

It is known that the number of the absorbed photons is directly related to the absorber volume [37,38]. Therefore, the amount of absorber material in all of the configurations in this

Optics EXPRESS

work is kept constant. Additionally, in order to account for the whole optically-active part of the absorber, the *optical thickness* is defined as the thickness from the top of the textures to the bottom of the absorber [38,39]. It should be noted that the optical thickness is different from the equivalent thickness (the ratio between the unit cell volume and its bottom area). Hence, the deviation of J_{ph} from Green limit for a CIGS slab with the same optical thickness can be calculated as [38]:

$$\Delta Green = \frac{J_{ph-CIGS} - J_{Green}}{J_{Green}}\% \tag{3}$$

where J_{Green} is the Green absorption limit integrated according to Eq. (1).

3. Results and discussion

3.1 Design considerations

As mentioned in the introduction, light management applied to both front and back of the solar cell can improve the optical performance of ultra-thin CIGS solar cells [4]. However, the parasitic absorption of the front layers and the optical shading caused by the front contact still hinder full usage of high energy photons. In this part, we suggest an IBC configuration to overcome those challenges and step by step investigate the design considerations.

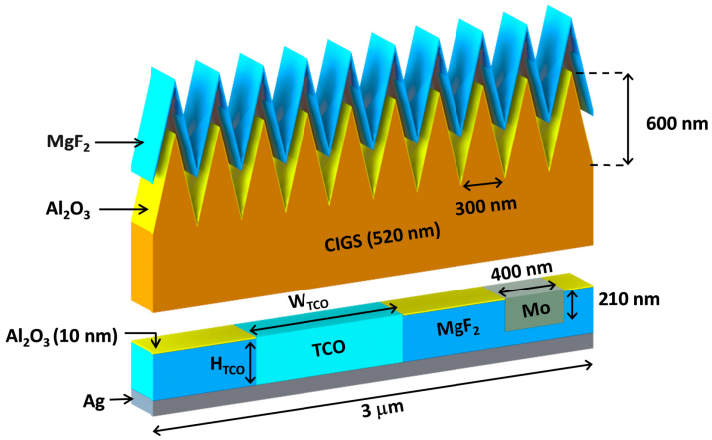

Fig. 1. Visual rendering of the back-contacted CIGS solar cell with high aspect ratio features at the front. W_{TCO} and H_{TCO} indicate, respectively, width and height of the TCO.

Optics EXPRESS

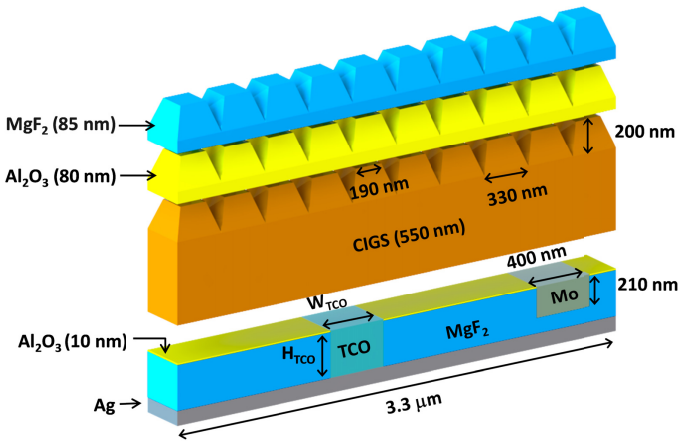

Fig. 2. Visual rendering of the back-contacted solar cell with natural CIGS morphology and optimized ARC. W_{TCO} and H_{TCO} indicate, respectively, width and height of the TCO.

First of all, note that in order to prevent the charge carrier recombination, the contact distance should be smaller than twice the minority carrier diffusion length. In case of a sub-micron thick CIGS layer, in which [Ga]/([Ga] + [In]) ratio (GGI) is almost uniform [40], the diffusion length is close to 1 µm [41-44], which is considered in our design platform.

In the IBC solar cell, the CIGS front surface should be chemically and preferably electrically passivated. This can be achieved by deploying an Al_2O_3 layer, either by atomic layer deposition (ALD) or by plasma-enhanced chemical vapor deposition (PECVD). The latter allows for higher growth rates and thicker layers of Al_2O_3. In both cases, the surface passivation quality can be significantly improved by annealing at 400-450 °C [45,46].

The antireflection effect can be realized by evaporating a layer of MgF_2 on the front side of the solar cell [47]. As the refractive index (n) of MgF_2 is lower than that of Al_2O_3, the grading in n from CIGS to that of air leads to a wideband antireflection effect.

At the rear side, the e- and h-contacts should be separated by a dielectric to avoid electrical shunts. In this case, MgF_2 with a high thermal resistivity [48] is chosen. A good chemical passivation will be guaranteed by the addition of a thin layer of Al_2O_3 onto the MgF_2 layer. Optically, the low refractive index of this dielectric stack increases the internal rear reflection and therefore improves the light's path length in the absorber [28].

A silver back reflector is placed at the rear side of the cell to ensure full internal rear reflection. This is merely to exclude the possible transmission losses from the optical performance in the model. Albeit, in practice, the cells can be fabricated on conventional soda lime glass [49,50] or flexible substrates [12,51] and a back reflector can be added to the rear side, if necessary.

Molybdenum is used for the h-contact, as it is proven to be inert, stands the high temperature fabrication process of CIGS and also forms with the absorber an ohmic contact for hole collection [52]. For the e-contact, an n-type transparent conductive oxide (TCO) should be selected to successfully collect the electrons. In our simulations, gallium-doped zinc oxide (GZO) type-a from [26] is used for this purpose. High carrier concentration, low free carrier absorption, transparency, high thermal stability and abundant constituting elements are the advantages of this material over other TCOs [26,31].

To ensure that charge carriers will be properly collected, an assessment of the band diagram of both contacts is necessary. Figure 3 shows the band diagram of the solar cell structure from the top Al_2O_3 layer to the e- and h-contacts. As can be seen in Fig. 3(b), at the front side, due to fixed negative charges in Al_2O_3 [53,54], an electric field, also known as front surface field [55] is formed in a way that allows accumulation of majority carriers, while repelling minority carriers at Al_2O_3/CIGS interface. The resulting electrical passivation

Optics EXPRESS

prevents minority charge carriers' recombination at the front side. At the rear side, high doping concentration makes GZO a degenerate semiconductor with a work function of about 4.26 eV. The resulting band bending inside CIGS forms a p-n junction in favor of electron collection and also hole repulsion. At the h-contact (Fig. 3(c)), Mo work-function (4.6 eV) enables an ohmic contact for CIGS majority carriers (holes) and therefore, their collection.

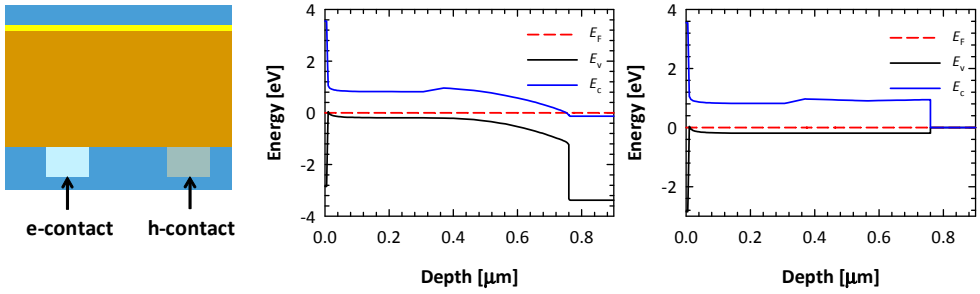

Fig. 3. a) Simplified layer stack of the e- and h-contacts in the envisioned IBC solar cell. From top to bottom: MgF_2, Al_2O_3, CIGS, GZO (e-contact on left-hand side) and Mo (h-contact on the right-hand side). Band diagrams in equilibrium b) and c) refer to e- and h-contact, respectively. E_F, E_v and E_c are Fermi, valance band edge and conduction band edge energies, respectively.

3.2 IBC solar cell with antireflective front textures

Figure 1 shows a visual rendering of the IBC CIGS solar cell. The presence of steep grooves with height to width ratio of 2 at the front side promotes light in-coupling and, hence, minimal reflection losses. As mentioned earlier, a thin layer of Al_2O_3 improves the chemical and electrical passivation of the front surface.

The height and width of GZO (H_{TCO} and W_{TCO}, respectively) were optimized for the best current density production. W_{TCO} was varied between 400 and 1000 nm in steps of 100 nm. H_{TCO} took values between 240 (30 nm thicker than Mo to ensure a gap between Mo and Ag) and 330 nm in steps of 30 nm. Figure 4(a) shows $J_{ph\text{-}CIGS}$ as a function of these parameters. Maximal $J_{ph\text{-}CIGS}$ can be obtained for $W_{TCO} > 800$ nm and $H_{TCO} > 290$ nm. Even though the optical performance might be better for larger W_{TCO}, we limited its range to values below the diffusion length to ensure good electrical performance as well. As a result, we selected 1000 nm and 320 nm as the optimal values for W_{TCO} and H_{TCO}, respectively. The absorptance and reflectance (1-R) spectra of the resulting configuration compared to the absorptance spectrum of the reference FBC solar cell is presented in Fig. 4(b). Owing to the elimination of front layers' parasitic absorption and the low reflectance, almost all of the incident high energy photons are absorbed by the CIGS layer. This leads to an improvement of J_{ph} from 28.04 mA/cm^2 for the reference cell to 39.69 mA/cm^2 for the IBC cell with optimal TCO (41.55% improvement). Using Eq. (3) to calculate ΔGreen for an optical thickness of 1120 nm (the peak-to-valley height of the textures plus the bulk thickness) shows that the IBC solar cell deviates from the benchmark by only 6.65%.

Optics EXPRESS

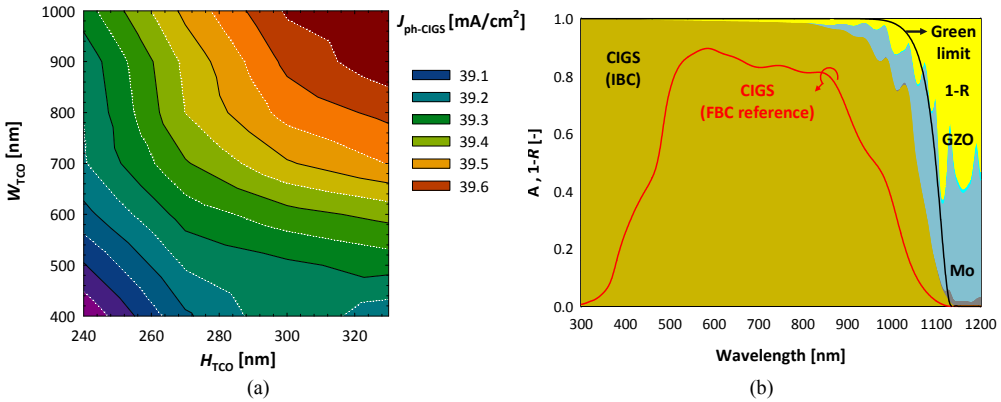

Fig. 4. a) Implied photocurrent density in CIGS layer ($J_{ph\text{-}CIGS}$) as a function of width and height of TCO. b) absorptance and 1-R spectra of the IBC solar cell when W_{TCO} = 1000 nm and H_{TCO} = 320 nm.

Even though the development of high aspect ratio textures on a CIGS layer is proven to be possible [56], this approach would need the partial removal of the absorber by ion bombardment [57] or wet etching [58]. This is in contrast with the photovoltaic (PV) market goal of increasing industrial throughput of CIGS PV technology by reducing material consumption [59-61]. In the following section, the development of the back-contacted solar cell with natural CIGS morphology is studied.

3.3 IBC solar cell with as-grown absorber morphology

According to our atomic force microscopy measurements for CIGS samples made at TNO [50], the lateral correlation length of the as-grown grains is about 330 nm [4,28]. This was included in the structure of a back-contacted CIGS solar cell model without antireflective textures (see Fig. 2). The natural roughness was modelled by introducing periodic truncated pyramids on the absorber bulk. Even though this is a simplification of the realistic device, the calibrated external quantum efficiency (EQE) and reflectance spectra sufficiently match the measured counterparts, confirming the validity of the assumption [28]. Note that the absorber volume in Figs. 1 and 2 are equal for fair comparison. In the absence of steep features at the front side for high light in-coupling, an alternative approach was employed. The thickness of passivating Al_2O_3 and antireflective MgF_2 layers in a reference solar cell were optimized for minimal reflection. The optimization algorithm is discussed in more details in [4]. The resulting thicknesses for Al_2O_3 and MgF_2 are 80 and 85 nm, respectively.

Performing the same TCO optimization procedure as in the previous session leads to the results shown in Fig. 5. $J_{ph\text{-}CIGS}$ values higher than 38.8 mA/cm^2 can be achieved for W_{TCO} > 950 nm and H_{TCO} > 300 nm. The optimal combination of these parameters (W_{TCO} = 1000 nm and H_{TCO} = 320 nm) resulted in the absorptance and 1-R spectra plotted in Fig. 5(b). As it can be seen in such a figure, a small drop in absorptance occurs at short wavelength region due to higher reflection from the front side of the cell. In total, $J_{ph\text{-}CIGS}$ = 38.84 mA/cm^2 is expected from the optimized cell, showing less than 0.9 mA/cm^2 decrease in $J_{ph\text{-}CIGS}$ compared to the previous design. Considering cheaper and easier fabrication process of this approach, the drop in $J_{ph\text{-}CIGS}$ appears negligible. In this case, where the optical thickness is 750 nm, J_{Green} = 42.11 mA/cm^2, and therefore, according to Eq. (3), ΔGreen will be 7.7%. This value is still very small compared to the case of the reference cell for which ΔGreen = 33.4%. The $J_{ph\text{-}CIGS}$ obtained in this work is comparable to the J_{sc} of world record efficiency CIGS solar cell [62], [63], in which parasitic absorption is still not addressed and the absorber thickness is considerably thicker than that of our design.

Optics EXPRESS

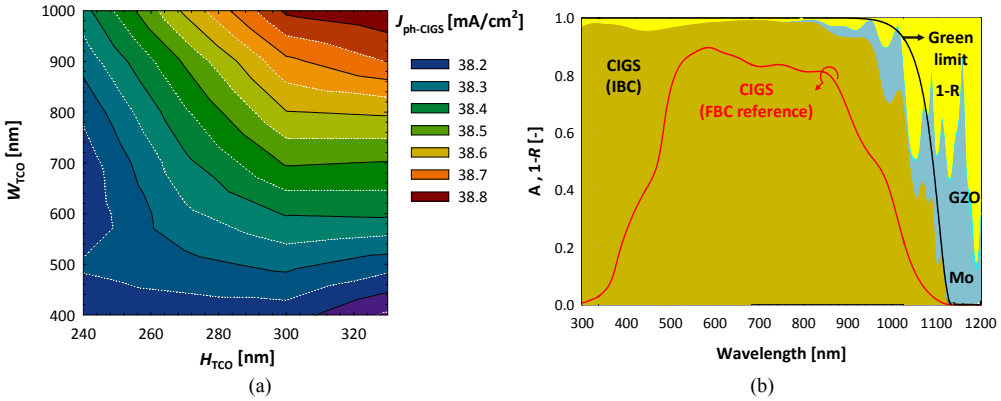

Fig. 5. a) Implied photocurrent density (J_{ph}) as a function of width and height of TCO. b) absorptance and 1-R spectra of the IBC solar cell when W_{TCO} = 1000 nm and H_{TCO} = 320 nm.

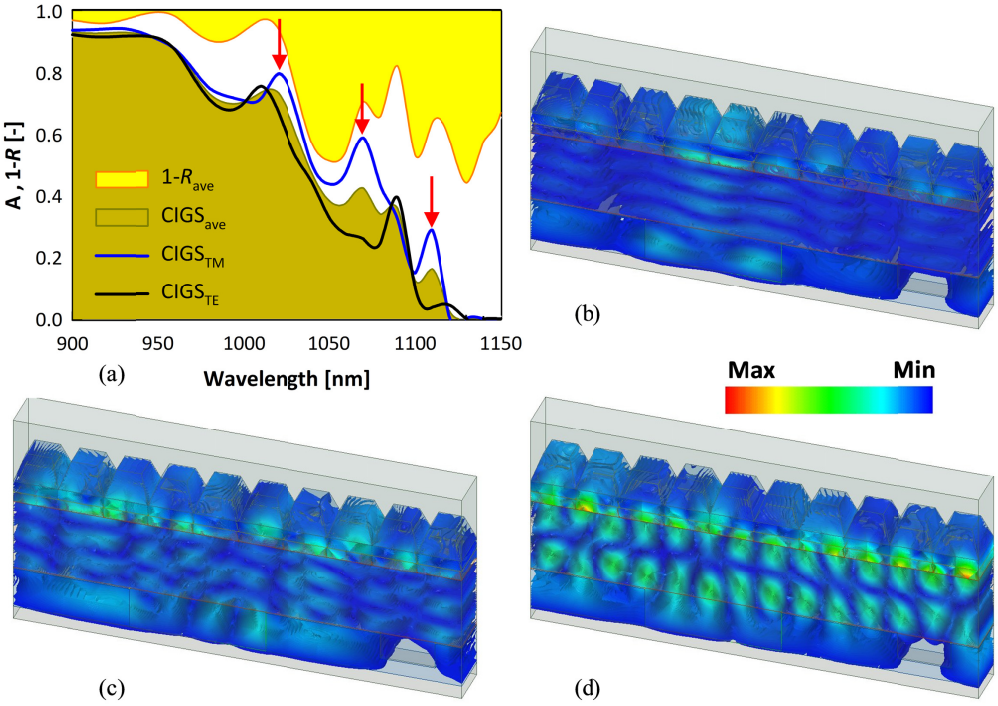

Fig. 6. a) CIGS absorption for TM (blue line), TE (black line) and average of TM and TE (brown area) polarizations and average 1-R (yellow area) spectra. The graphs correspond to the optimized IBC solar cell with as-grown CIGS grains. b) – d) Electric field magnitude at wavelength b) 1020 nm, c) 1070 nm and d) 1110 nm for TM polarization corresponding to local maxima in CIGS absorption, also indicated with red arrows in a).

We analyzed the optical performance of the IBC cell in more details for wavelengths longer than 900 nm. Figure 6(a) shows a close-up of Fig. 5(b) overlaid by TM and TE components of the absorptance spectrum. As can be seen in this figure, the wavelength and amplitude of the average CIGS absorptance in low-energy part of the spectrum is mainly dominated by TM polarization. Figures 6(b)-6(d) present the electric field magnitude ($\left|\vec{E}\right|$) at wavelengths corresponding to three local maxima in the TM-polarized absorptance spectrum.

These maxima are located at wavelengths 1020, 1070 and 1110 nm, indicated with red arrows in Fig. 6(a). It should be noted that each local maximum in CIGS absorptance is correlated with a local minimum in total reflectance. This means that as more photons are trapped in the solar cell bulk, less photons escape from the cell. At 1020 nm (Fig. 6(b)), the Fabry-Perót modes are the main components of the electric field, causing the light to mainly propagate in perpendicular direction with respect to the plane of incidence [64]. As the wavelength increases, the diffraction modes triggered by the rear dielectric/metal IBC arrangement (GZO / MgF_2 / Mo / MgF_2) and coupled with waveguide modes inside the absorber bulk outweigh the Fabry-Perót modes. This phenomenon is clearly visible in Figs. 6(c) and 6(d), where waveguide modes are the dominant components of the electric field.

Even though the CIGS absorptance might have a slightly different shape in the two IBC designs in the long-wavelength regime (see Fig. 4(b) and Fig. 5(b)), the total generated J_{ph} in that part is not very different. For instance, for wavelengths between 900 and 1200 nm, the obtained J_{ph}'s from the first and the second IBC structures are 7.09 and 6.62 mA/cm^2, respectively. This is due to the limited capability of the absorber in absorbing close-to-bandgap photons. Therefore, the higher intensity of the electric field in Fig. 6(d) does not necessarily mean that the absorber will be capable of absorbing all of the trapped photons.

It should be noted that we also considered ITO as e-contact material in our models. In that case, due to the lower transparency of ITO material [26], less $J_{ph\text{-}CIGS}$ can be expected by the optimized structure. More importantly, the presence of indium in ITO contradicts our goal of decreasing indium usage and thus fabricating cost-effective CIGS solar cells. Hence, we excluded ITO from our proposed IBC structure.

4. Conclusions

CIGS with a low bandgap and high absorption coefficient, is a great candidate for thin-film solar cell applications. High parasitic absorption in front/back-contacted solar cell architectures hinders the full utilization of CIGS's optical potential. In this work a back-contacted CIGS solar cell was proposed. The assessment of electron- and hole-contacts' band diagram shows well-functioning structure from electrical point of view. An IBC cell with antireflective textures and optimized TCO dimensions showed a potential 41.55% improvement in implied photocurrent density ($J_{ph\text{-}CIGS}$) compared to a front/back-contacted reference cell. A simpler structure with as-grown CIGS morphology and optimized flat antireflection coating revealed a maximum $J_{ph\text{-}CIGS}$ value of 38.84 mA/cm^2. This value deviates from the theoretical Green limit by only 7.7% and is comparable to the short circuit current density of the world record CIGS solar cell, albeit with significantly thicker absorber.

Even though the fabrication of our proposed IBC structure in the current design might be complicated, eventually including a number of etching and lithography steps, we believe that this is an important step towards the development of high efficiency and cost-effective CIGS solar cells. More theoretical and experimental studies are needed to reach a balance between the cost and efficiency of such devices.

References

1. B. Vermang, J. T. Wätjen, V. Fjällström, F. Rostvall, M. Edoff, R. Gunnarsson, I. Pilch, U. Helmersson, R. Kotipalli, F. Henry, and D. Flandre, "Highly reflective rear surface passivation design for ultra-thin Cu(In,Ga)Se_2 solar cells," Thin Solid Films **582**, 300–303 (2015).
2. L. M. Mansfield, A. Kanevce, S. P. Harvey, K. Bowers, C. Beall, S. Glynn, and I. L. Repins, "Efficiency increased to 15.2% for ultra-thin Cu(In,Ga)Se_2 solar cells," Prog. Photovolt. Res. Appl. **26**(11), 949–954 (2018).
3. G. Yin, P. Manley, and M. Schmid, "Light trapping in ultrathin CuIn1-xGaxSe_2 solar cells by dielectric nanoparticles," Sol. Energy **163**, 443–452 (2018).
4. N. Rezaei, O. Isabella, Z. A. E. P. Vroon, and M. Zeman, "Optical optimization of a multi-layer wideband anti-reflection coating using porous MgF_2 for sub-micron-thick CIGS solar cells," Sol. Energy **177**, 59–67 (2019).
5. S. Hwang and J.-H. Jang, "3D simulations for the optimization of antireflection subwavelength structures in CIGS solar cells," in Photovoltaic Specialists Conference (PVSC), 2012 38th IEEE, 864–867, IEEE, (2012).
6. L. Aé, D. Kieven, J. Chen, R. Klenk, T. Rissom, Y. Tang, and M. C. Lux-Steiner, "ZnO nanorod arrays as an antireflective coating for Cu (In, Ga) Se_2 thin film solar cells," Prog. Photovolt. Res. Appl. **18**(3), 209–213

Optics EXPRESS

(2010).
7. J. Krc, M. Sever, A. Campa, Z. Lokar, B. Lipovsek, and M. Topic, "Optical confinement in chalcopyrite based solar cells," Thin Solid Films **633**, 193–201 (2016).
8. M. Schmid, P. Manley, A. Ott, M. Song, and G. Yin, "Nanoparticles for light management in ultrathin chalcopyrite solar cells," J. Mater. Res. **31**(21), 3273–3289 (2016).
9. B. Vermang, J. T. Wätjen, V. Fjällström, F. Rostvall, M. Edoff, R. Gunnarsson, I. Pilch, U. Helmersson, R. Kotipalli, F. Henry, and D. Flandre, "Highly reflective rear surface passivation design for ultra-thin Cu (In, Ga) Se_2 solar cells," Thin Solid Films **582**, 300–303 (2015).
10. C. Onwudinanti, R. Vismara, O. Isabella, L. Grenet, F. Emieux, and M. Zeman, "Advanced light management based on periodic textures for Cu(In,Ga)Se_2 thin-film solar cells," Opt. Express **24**(6), A693–A707 (2016).
11. J. Goffard, C. Colin, F. Mollica, A. Cattoni, C. Sauvan, P. Lalanne, J.-F. Guillemoles, N. Naghavi, and S. Collin, "Light trapping in ultrathin CIGS solar cells with nanostructured back mirrors," IEEE J. Photovolt. **7**(5), 1433–1441 (2017).
12. R. Kaczynski, J. Lee, J. van Alsburg, B. Sang, U. Schoop, and J. Britt, "In-line Potassium Fluoride Treatment of CIGS Absorbers Deposited on Flexible Substrates in a Production-Scale Process Tool," in IEEE PVSC, 1455–1458, IEEE, (2017).
13. M. D. Lammert and R. J. Schwartz, "The interdigitated back contact solar cell: a silicon solar cell for use in concentrated sunlight," IEEE Trans. Electron Dev. **24**(4), 337–342 (1977).
14. P. Procel, A. Ingenito, R. De Rose, S. Pierro, F. Crupi, M. Lanuzza, G. Cocorullo, O. Isabella, and M. Zeman, "Opto-electrical modelling and optimization study of a novel IBC c-Si solar cell," Prog. Photovolt. Res. Appl. **25**(6), 452–469 (2017).
15. G. Yang, P. Guo, P. Procel, G. Limodio, A. Weeber, O. Isabella, and M. Zeman, "High-efficiency black IBC c-Si solar cells with poly-Si as carrier-selective passivating contacts," Sol. Energy Mater. Sol. Cells **186**, 9–13 (2018).
16. D. D. Smith, G. Reich, M. Baldrias, M. Reich, N. Boitnott, and G. Bunea, "Silicon solar cells with total area efficiency above 25%," in Photovoltaic Specialists Conference (PVSC), 2016 IEEE 43rd, 3351–3355, IEEE, (2016).
17. P. Wagner, J. C. Stang, M. Mews, A. B. Morales-Vilches, B. Stannowski, B. Stegemann, and L. Korte, "Interdigitated back contact silicon heterojunction solar cells: Towards an industrially applicable structuring method," AIP Conf. Proc. **1999**, 60001 (2018).
18. A. Tomasi, B. Paviet-Salomon, Q. Jeangros, J. Haschke, G. Christmann, L. Barraud, A. Descoeudres, J. P. Seif, S. Nicolay, M. Despeisse, S. De Wolf, and C. Ballif, "Simple processing of back-contacted silicon heterojunction solar cells using selective-area crystalline growth," Nat. Energy **2**(5), 17062 (2017).
19. K. Yoshikawa, H. Kawasaki, W. Yoshida, T. Irie, K. Konishi, K. Nakano, T. Uto, D. Adachi, M. Kanematsu, H. Uzu, and K. Yamamoto, "Silicon heterojunction solar cell with interdigitated back contacts for a photoconversion efficiency over 26%," Nat. Energy **2**(5), 17032 (2017).
20. F. Haase, C. Hollemann, S. Schäfer, A. Merkle, M. Rienäcker, J. Krügener, R. Brendel, and R. Peibst, "Laser contact openings for local poly-Si-metal contacts enabling 26.1%-efficient POLO-IBC solar cells," Sol. Energy Mater. Sol. Cells **186**, 184–193 (2018).
21. K. Masuko, M. Shigematsu, T. Hashiguchi, D. Fujishima, M. Kai, N. Yoshimura, T. Yamaguchi, Y. Ichihashi, T. Mishima, N. Matsubara, T. Yamanishi, T. Takahama, M. Taguchi, E. Maruyama, and S. Okamoto, "Achievement of more than 25% conversion efficiency with crystalline silicon heterojunction solar cell," IEEE J. Photovolt. **4**(6), 1433–1435 (2014).
22. J. Nakamura, N. Asano, T. Hieda, C. Okamoto, H. Katayama, and K. Nakamura, "Development of heterojunction back contact Si solar cells," IEEE J. Photovolt. **4**(6), 1491–1495 (2014).
23. Synopsys, *Sentaurus Device User* (2014).
24. P. Procel, G. Yang, O. Isabella, and M. Zeman, "Theoretical evaluation of contact stack for high efficiency IBC-SHJ solar cells," Sol. Energy Mater. Sol. Cells **186**(May), 66–77 (2018).
25. J. Pettersson, C. Platzer-Björkman, U. Zimmermann, and M. Edoff, "Baseline model of graded-absorber Cu(In,Ga)Se_2 solar cells applied to cells with Zn1−xMgxO buffer layers," Thin Solid Films **519**(21), 7476–7480 (2011).
26. H. Fujiwara and M. Kondo, "Effects of carrier concentration on the dielectric function of ZnO:Ga and In_2O_3:Sn studied by spectroscopic ellipsometry: Analysis of free-carrier and band-edge absorption," Phys. Rev. B Condens. Matter Mater. Phys. **71**(7), 75109 (2005).
27. G. Dingemans and W. M. M. Kessels, "Status and prospects of Al_2O_3-based surface passivation schemes for silicon solar cells," J. Vac. Sci. Technol. A **30**(4), 040802 (2012). https://doi.org/10.1116/1.4728205.
28. N. Rezaei, O. Isabella, Z. Vroon, and M. Zeman, "Quenching Mo optical losses in CIGS solar cells by a point contacted dual-layer dielectric spacer: a 3-D optical study," Opt. Express **26**(2), A39–A53 (2018).
29. R. Vismara, O. Isabella, and M. Zeman, "Back-contacted $BaSi_2$ solar cells: an optical study," Opt. Express **25**(8), A402–A408 (2017).
30. O. Isabella, S. Solntsev, D. Caratelli, and M. Zeman, "3-D optical modeling of thin-film silicon solar cells on diffraction gratings," Prog. Photovolt. Res. Appl. **21**(1), 94–108 (2013).
31. O. Isabella, H. Sai, M. Kondo, and M. Zeman, "Full-wave optoelectrical modeling of optimized flattened light-scattering substrate for high efficiency thin-film silicon solar cells," Prog. Photovolt. Res. Appl. **22**(6), 671–689 (2014).

Optics EXPRESS

32. O. Lundberg, M. Bodegård, J. Malmström, and L. Stolt, "Influence of the Cu(In,Ga)Se_2 thickness and Ga grading on solar cell performance," Prog. Photovolt. Res. Appl. **11**(2), 77–88 (2003).
33. C. Onwudinanti, R. Vismara, O. Isabella, L. Grenet, F. Emieux, and M. Zeman, "Advanced light management based on periodic textures for Cu(In,Ga)Se_2 thin-film solar cells," Opt. Express **24**(6), A693–A707 (2016).
34. M. J. Dodge, "Refractive properties of magnesium fluoride," Appl. Opt. **23**(12), 1980–1985 (1984).
35. NREL, "Reference solar spectral irradiance: air mass 1.5," <https://www.nrel.gov/grid/solar-resource/spectra.html>.
36. M. A. Green, "Lambertian light trapping in textured solar cells and light-emitting diodes: Analytical solutions," Prog. Photovolt. Res. Appl. **10**(4), 235–241 (2002).
37. K. X. Wang, Z. Yu, V. Liu, Y. Cui, and S. Fan, "Absorption enhancement in ultrathin crystalline silicon solar cells with antireflection and light-trapping nanocone gratings," Nano Lett. **12**(3), 1616–1619 (2012).
38. O. Isabella, R. Vismara, D. N. P. Linssen, K. X. Wang, S. Fan, and M. Zeman, "Advanced light trapping scheme in decoupled front and rear textured thin-film silicon solar cells," Sol. Energy **162**, 344–356 (2018).
39. C. S. Schuster, A. Bozzola, L. C. Andreani, and T. F. Krauss, "How to assess light trapping structures versus a Lambertian Scatterer for solar cells?" Opt. Express **22**(S2 Suppl 2), A542–A551 (2014).
40. E. Jarzembowski, M. Maiberg, F. Obereigner, K. Kaufmann, S. Krause, and R. Scheer, "Optical and electrical characterization of Cu (In, Ga) Se_2 thin film solar cells with varied absorber layer thickness," Thin Solid Films **576**, 75–80 (2015).
41. G. Brown, V. Faifer, A. Pudov, S. Anikeev, E. Bykov, M. Contreras, and J. Wu, "Determination of the minority carrier diffusion length in compositionally graded Cu(In, Ga)Se_2 solar cells using electron beam induced current," Appl. Phys. Lett. **96**(2), 22104 (2010).
42. T. Hara, T. Maekawa, S. Minoura, Y. Sago, S. Niki, and H. Fujiwara, "Quantitative Assessment of Optical Gain and Loss in Submicron-Textured CuIn 1−x Ga x Se_2 Solar Cells Fabricated by Three-Stage Coevaporation," Phys. Rev. Appl. **2**(3), 34012 (2014).
43. O. Lundberg, M. Edoff, and L. Stolt, "The effect of Ga-grading in CIGS thin film solar cells," Thin Solid Films **480**, 520–525 (2005).
44. R. Kniese, M. Powalla, and U. Rau, "Evaluation of electron beam induced current profiles of Cu(In,Ga)Se_2 solar cells with different Ga-contents," Thin Solid Films **517**(7), 2357–2359 (2009).
45. B. Macco, "Atomic layer deposition of metal oxide thin films for Si heterojunction solar cells," Technische Universiteit Eindhoven (2016).
46. G. Dingemans, M. C. M. van de Sanden, and W. M. M. Kessels, "Influence of the Deposition Temperature on the c-Si Surface Passivation by Al_2O_3 Films Synthesized by ALD and PECVD," Electrochem. Solid-State Lett. **13**(3), H76 (2010).
47. P. Jackson, R. Wuerz, D. Hariskos, E. Lotter, W. Witte, and M. Powalla, "Effects of heavy alkali elements in Cu(In,Ga)Se_2 solar cells with efficiencies up to 22.6%," Phys. Status Solidi-R **10**(8), 583–586, Wiley Online Library (2016).
48. J. D. Bass, C. Boissiere, L. Nicole, D. Grosso, and C. Sanchez, "Thermally Induced Porosity in CSD MgF_2-Based Optical Coatings: An Easy Method to Tune the Refractive Index," Chem. Mater. **20**(17), 5550–5556 (2008).
49. I. Repins, M. A. Contreras, B. Egaas, C. DeHart, J. Scharf, C. L. Perkins, B. To, and R. Noufi, "19· 9%□ efficient ZnO/CdS/CuInGaSe_2 solar cell with 81· 2% fill factor," Prog. Photovolt. Res. Appl. **16**(3), 235–239 (2008).
50. A. J. Blanker, P. Berendsen, N. Phung, Z. Vroon, M. Zeman, and A. H. M. Smets, "Advanced light management techniques for two-terminal hybrid tandem solar cells," Sol. Energy Mater. Sol. Cells **181**, 77–82 (2018).
51. D. J. Hwang, S. Kuk, Z. Wang, S. Fu, T. Zhang, G. Kim, W. M. Kim, and J.-H. Jeong, "Laser scribing of CIGS thin-film solar cell on flexible substrate," Appl. Phys. A **123**(1), 55 (2017).
52. K. Orgassa, H. W. Schock, and J. H. Werner, "Alternative back contact materials for thin film Cu (In, Ga) Se_2 solar cells," Thin Solid Films **431**, 387–391 (2003).
53. R. Kotipalli, B. Vermang, J. Joel, R. Rajkumar, M. Edoff, and D. Flandre, "Investigating the electronic properties of Al_2O_3 Cu(In,Ga)Se_2 interface," AIP Adv. **5**(10), 107101 (2015).
54. B. Macco, B. W. H. van de Loo, and W. M. M. Kessels, "Atomic Layer Deposition for High Efficiency Crystalline Silicon Solar Cells," in Atomic Layer Deposition in Energy Conversion Applications, pp. 41–99, Wiley-VCH Verlag (2017).
55. A. Ingenito, O. Isabella, and M. Zeman, "Nano□cones on micro□pyramids: modulated surface textures for maximal spectral response and high□efficiency solar cells," Prog. Photovolt. Res. Appl. **23**(11), 1649–1659 (2015).
56. S. R. Thomas, C.-W. Chen, M. Date, Y.-C. Wang, H.-W. Tsai, Z. M. Wang, and Y.-L. Chueh, "Recent developments in the synthesis of nanostructured chalcopyrite materials and their applications: a review," RSC Advances **6**(65), 60643–60656 (2016).
57. C. H. Liu, C. H. Chen, S. Y. Chen, Y. T. Yen, W. C. Kuo, Y. K. Liao, J. Y. Juang, H. C. Kuo, C. H. Lai, L. J. Chen, and Y. L. Chueh, "Large scale single-crystal Cu(In,Ga)Se_2 nanotip arrays for high efficiency solar cell," Nano Lett. **11**(10), 4443–4448 (2011).
58. W. N. Shafarman, R. S. Huang, and S. H. Stephens, "Characterization of Cu(InGa)Se2 solar cells using etched absorber layers," Conf. Rec. 2006 IEEE 4th World Conf. Photovolt. Energy Conversion, WCPEC-4 **1**, 420–423, IEEE (2007).

Optics EXPRESS

59. F. Mollica, J. Goffard, M. Jubault, F. Donsanti, S. Collin, A. Cattoni, L. Lombez, N. Naghavi, R. Edf, I. Umr, and D. Renaissance, "Comparative study of patterned TiO 2 and Al 2 O 3 layers as passivated back-contact for ultra-thin Cu (In, Ga)Se_2 solar cells," in Photovoltaic Specialists Conference (PVSC), 2016 IEEE 43rd, 6–10, IEEE, (2016).
60. Z. Jehl, F. Erfurth, N. Naghavi, L. Lombez, I. Gerard, M. Bouttemy, P. Tran-Van, A. Etcheberry, G. Voorwinden, B. Dimmler, W. Wischmann, M. Powalla, J. F. Guillemoles, and D. Lincot, "Thinning of CIGS solar cells: Part II: Cell characterizations," Thin Solid Films **519**(21), 7212–7215 (2011).
61. M. Schmid, "Review on light management by nanostructures in chalcopyrite solar cells," Semicond. Sci. Technol. **32**(4), 43003 (2017).
62. "Solar Frontier Achieves World Record Thin-Film Solar Cell Efficiency of 22.9%," 2017, <http://www.solar-frontier.com/eng/news/2017/1220_press.html>.
63. Y. Hishikawa, E. D. Dunlop, M. A. Green, J. Hohl, E. Anita, W. Y. H. Baillie, and D. H. Levi, "Solar cell efficiency tables (version 52)," 427–436 (2018).
64. R. Vismara, O. Isabella, A. Ingenito, F. T. Si, and M. Zeman, "Geometrical optimisation of core-shell nanowire array for enhanced absorption in thin crystalline silicon heterojunction solar cells," Beilstein J. Nanotechnol. **10**, 322-331 (2019).